

Title No. 116-S93

Mixed-Type Modeling of Structures with Slender and Deep Beam Elements

by Jian Liu, Serhan Guner, and Boyan I. Mihaylov

The nonlinear analysis of reinforced concrete frame structures with slender members can be performed accurately and efficiently with one-dimensional (1-D) elements based on the plane-sections-remain-plane hypothesis. However, if the frame also includes deep beams which require two-dimensional (2-D) high-fidelity finite element procedures, the analysis of large structures can become very costly. To address this challenge, this paper proposes a mixed-type modeling framework which integrates 1-D slender beam elements with a novel 1-D macroelement for deep beams. The framework is implemented in an existing nonlinear analysis procedure and is used to model 18 deep beam tests and a 20-story frame. It is shown that the proposed modeling framework provides similarly accurate predictions to the 2-D high-fidelity procedures but requires a fraction of the time for modeling and analysis. Furthermore, the macroelement improves the post-peak predictions, and therefore the framework is suitable for evaluating the resilience of structures under extreme loading.

Keywords: deep beams; macroelement; mixed-type modeling; shear; slender elements.

INTRODUCTION

Deep beams are characterized by small shear span-depth ratios and carry shear by direct compression between the loading and support points (known as the strut or arch action). As concrete is very efficient in resisting compression, such members possess high stiffness and shear strengths as compared to slender beams. Owing to these properties, deep beams are typically used as transfer girders above large open spaces in the bottom floors of important concrete buildings such as government centers, hospitals, and high-rise buildings (Fig. 1). The load-bearing characteristics of deep beams are also encountered in other members such as spread footings and pile caps. Due to their important functions, deep beams may often dictate the resilience of the entire structure when overloading occurs in rare events. The 2011 Christchurch earthquake, for example, produced unforeseen vertical ground accelerations (up to 1.8g) and caused the shear failures of several deep transfer girders. As a result, a number of buildings were on the verge of collapse and had to be demolished in the months after the earthquake.¹⁻⁴

To design structures for resilience to extreme loading events, it is often necessary to perform a nonlinear pushover analysis, with the entire structure subjected to, for example, an earthquake or a column removal scenario representing a blast or impact loading.⁵ Two approaches are commonly used for modeling buildings, which incorporate deep transfer girders. The most common strategy, shown on the left in Fig. 1, is to model all members with one-dimensional (1-D) slender elements based on the classical plane-sections-remain-plane hypothesis (fiber-based elements or lumped plas-

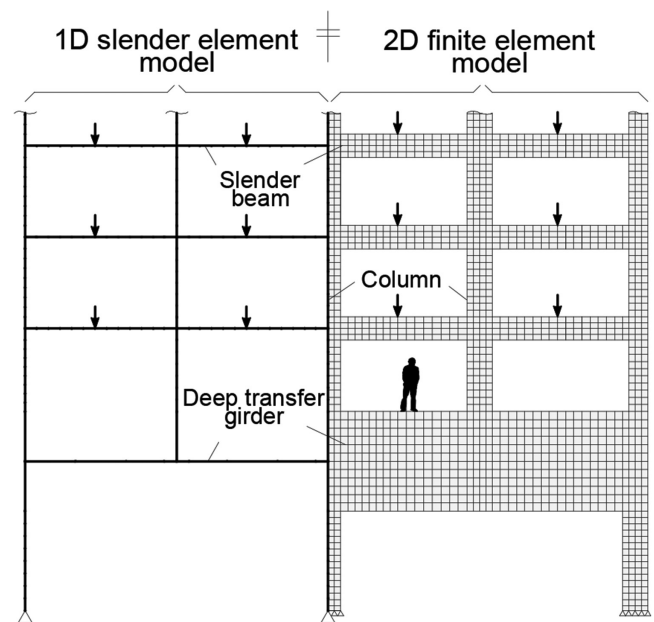


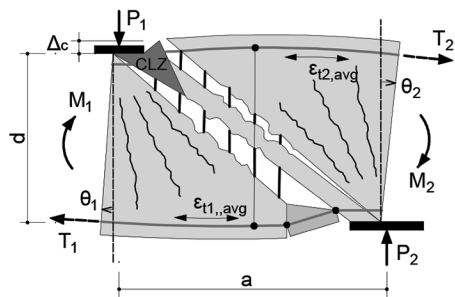
Fig. 1—Alternative models of large four-bay frame structure with both slender and deep beams.

ticity elements). This approach neglects the complex behavioral mechanisms associated with deep beams and cannot capture the interaction and redistribution of internal forces between the deep and slender members. While incorrect, this strategy is still commonly used due to its relatively simple and computationally efficient nature. The second approach is to use two-dimensional (2-D) nonlinear finite element methods (FEMs) which incorporate appropriate constitutive models for cracked reinforced concrete under plane stresses.⁶ This approach captures the strut action of deep beams, the interaction between deep and slender elements, and the force redistribution in the post-peak stages. The disadvantage of 2-D FEMs is that they require significant knowledge and experience from the user and demand significant time for the model development and analysis execution. Consequently, they are feasible only when modeling critical parts of structures as opposed to an entire building. A few other modeling frameworks—for example, hybrid modeling⁷—are also available, which combines these two modeling approaches.

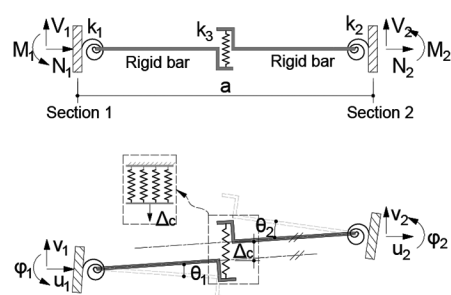
This paper proposes a mixed-type modeling framework which aims to combine the accuracy of 2-D FEMs with the

ACI Structural Journal, V. 116, No. 4, July 2019.

MS No. S-2018-329, doi: 10.14359/51715632, was received August 3, 2018, and reviewed under Institute publication policies. Copyright © 2019, American Concrete Institute. All rights reserved, including the making of copies unless permission is obtained from the copyright proprietors. Pertinent discussion including author's closure, if any, will be published ten months from this journal's date if the discussion is received within four months of the paper's print publication.



a) Three-parameter kinematic model



b) Components and deformed shape of macroelement

Fig. 2—Macroelement for shear spans of deep beams.

speed and simplicity of 1-D slender elements. The framework integrates 1-D slender beam elements with equally simple 1-D deep beam elements that can account for the strut action. The deep beam element incorporated in this study was recently formulated by Liu and Mihaylov⁸ based on a three-parameter kinematic theory⁹ for continuous deep beams. This element can capture the entire nonlinear shear response of deep shear spans, from initial high stiffnesses to the post-peak response, which provides the structure with the ability to redistribute forces and survive overloading. The paper discusses the formulation of the proposed mixed-type modeling framework, provides comparisons with experimental tests, and presents a sample analysis of an entire 20-story frame with deep transfer girders.

RESEARCH SIGNIFICANCE

The evaluation of the resilience of large frame structures with deep transfer girders requires modeling the interaction between the deep girders and the rest of the structure in an accurate and computationally effective manner. This paper proposes a mixed-type modeling framework that combines commonly used 1-D slender beam elements with a novel and equally simple 1-D deep beam element to accurately account for failures and post-peak behaviors associated with complex shear failures. The new nonlinear modeling framework requires a fraction of the computational time required by 2-D approaches while capturing the complete response of structures with a comparable accuracy.

1-D MACROELEMENT FOR DEEP BEAMS

The efficient modeling of slender beams can be accomplished based on the plane-sections-remain-plane hypoth-

esis, which greatly simplifies the deformation patterns without compromising accuracy. To model deep beams in a similar fashion, it is necessary to describe their apparently complex deformation patterns in a simple and sufficiently accurate manner.

Figure 2(a) shows such a model for deep beams under double curvature proposed by Mihaylov et al.⁹ In this model, a shear span of a deep beam is divided into two parts by a critical diagonal crack. Each of the parts is modeled as a “fan” of rigid struts outlined by radial cracks. The struts are pinned at points P_1 and P_2 and are connected to the bottom/top flexural reinforcement, respectively. As the flexural reinforcement develops average tensile strains $\epsilon_{t1,avg}$ and $\epsilon_{t2,avg}$ along the shear span a , the fans “open” by angles θ_1 and θ_2 . While these deformations can be associated with flexure, the shear force causes the two fans to translate vertically with respect to each other due to the opening of the critical diagonal crack. The vertical displacement Δ_c in the crack is associated with diagonal crushing of the concrete in the critical loading zone (CLZ). Based on these kinematic assumptions, the complete displacement field of the shear span can be expressed as a function of only three degrees of freedom: $\epsilon_{t1,avg}$, $\epsilon_{t2,avg}$, and Δ_c , or eventually θ_1 , θ_2 , and Δ_c .

This three-parameter kinematic model forms the basis of the macroelement for deep beams proposed by Liu and Mihaylov⁸ (Fig. 2(b)). In this element, the behavior of the two fans is modeled by rotational springs, while the shear behavior across the critical diagonal crack is represented by a transverse spring. The rotational springs are attached to end sections/nodes with two translational and one rotational degrees of freedom per node (u , v , ϕ). Inside the element, the three springs are connected by bars that are rigid in flexure and remain parallel to each other as the element deforms.

The nonlinear load-deformation relationships $M_i(\theta_i)$ and $V(\Delta_c, \theta_i)$ of the springs of the macroelement are developed from first principles: compatibility of deformations, stress-strain relationships, and equilibrium. For a given degree of freedom (DOF) θ_1 , the average strain in the bottom longitudinal reinforcement $\epsilon_{t1,avg}$ is determined from compatibility. Using this strain, the tensile force in the reinforcement T_1 is determined by assuming an elastic-perfectly-plastic stress-strain relationship for the reinforcement, and also adding the tension-stiffening effect of the concrete around the reinforcement. The bending moment M_1 is then obtained from equilibrium as $T_1(0.9d)$, where d is the effective depth of the section and $0.9d$ (Reference 10) is the estimated lever arm of the internal longitudinal forces. A schematic representation of the $M_i(\theta_i)$ relationship obtained in this manner is shown in Fig. 3(a).⁸

The $V(\Delta_c, \theta_i)$ relationship of the transverse spring is somewhat more complex due to the complex manner in which deep beams resist shear. The macroelement accounts for four mechanisms of shear resistance across the critical diagonal crack: 1) shear carried in the critical loading zone, V_{CLZ} ; 2) tension in the transverse reinforcement, V_s ; 3) aggregate interlock shear, V_{ci} ; and 4) dowel action of the longitudinal reinforcement, V_d . Therefore, the transverse spring can be visualized as consisting of four parallel springs, where the strut action is associated mainly with spring V_{CLZ} .

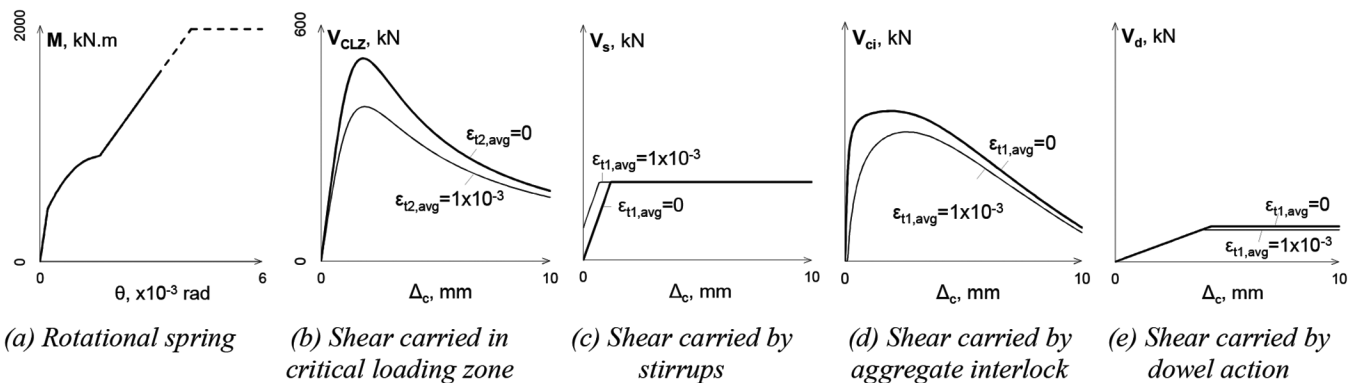


Fig. 3—Load-deformation relationships of springs of macroelement. (Note: Plots are prepared based on Beam SIM by Mihaylov et al.¹¹ with $a/d = 1.55$, $d = 1095$ mm, $b = 400$ mm, $l_{bl} = 300$ mm, $\rho_l = 0.70\%$, $\rho_v = 0.10\%$, and $f'_c = 33.0$ MPa; 1 mm = 0.039 in.; 1 m = 3.28 ft; 1 kN = 0.225 kip; 1 MPa = 145.038 psi.)

The constitutive relationships of the four springs are presented schematically in Fig. 3(b) through (e). As evident from the plots, the behavior of the CLZ resembles that of concrete in compression, while the behavior of the stirrups is similar to the tensile behavior of steel. To model the aggregate interlock spring, it is necessary to use DOFs Δ_c and θ_1 (or $\epsilon_{t1,avg}$) as they both contribute to the relative displacements between the crack faces. For given values of these DOFs, the average width of the critical crack w and the slip displacement s are expressed using the kinematic model. DOF θ_1 results in the widening of the critical crack while Δ_c causes both widening and slip. Displacements w and s are used to calculate the aggregate interlock stress on the crack $v_{ci}(w, s)$ based on a contact density model by Li et al.,¹² and v_{ci} is integrated along the critical crack to obtain the shear force V_{ci} . As can be seen from Fig. 3(d), V_{ci} increases with increasing Δ_c and eventually diminishes as the critical crack becomes very wide. At the bottom of the crack, the longitudinal reinforcement works in double curvature associated with DOF Δ_c , and therefore resists shear by dowel action. By modeling the bars in this zone as fixed-fixed steel beams, the dowel action relationship in Fig. 3(e) has been obtained. The dowel action is diminished by the tensile strain in the reinforcement $\epsilon_{t1,avg}$.

To solve the nonlinear equations of the macroelement, a secant stiffness approach is employed, which will provide compatibility with the existing 1-D slender beam elements. Therefore, the stiffnesses of the three springs of the element are obtained as $k_1 = M_1/\theta_1$, $k_2 = M_2/\theta_2$, and $k_3 = V/\Delta_c$, and the secant stiffness matrix is formulated as

$$\begin{Bmatrix} N_1 \\ V_1 \\ M_1 \\ N_2 \\ V_2 \\ M_2 \end{Bmatrix} = [k] \begin{Bmatrix} u_1 \\ v_1 \\ \phi_1 \\ u_2 \\ v_2 \\ \phi_2 \end{Bmatrix} \quad (1)$$

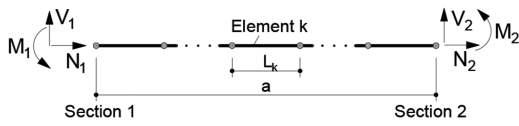
$$[k] = \frac{1}{C} \times \begin{bmatrix} CE_c A_g / a & 0 & 0 & -CE_c A_g / a & 0 & 0 \\ 0 & k_3(k_1 + k_2) & k_1 k_3 a & 0 & -k_3(k_1 + k_2) & k_2 k_3 a \\ 0 & k_1 k_3 a & k_1(k_2 + k_3 a^2) & 0 & -k_1 k_3 a & -k_1 k_2 \\ -CE_c A_g / a & 0 & 0 & CE_c A_g / a & 0 & 0 \\ 0 & -k_3(k_1 + k_2) & -k_1 k_3 a & 0 & k_3(k_1 + k_2) & -k_2 k_3 a \\ 0 & k_2 k_3 a & -k_1 k_2 & 0 & -k_2 k_3 a & k_2(k_1 + k_3 a^2) \end{bmatrix} \quad (2)$$

where $C = k_1 + k_2 + k_3 a$ (Reference 2); a is the shear span; E_c is the modulus of elasticity of the concrete; and A_g is the gross area of the concrete section. This matrix is an extension of the formulation presented in Liu and Mihaylov,⁸ which did not account for the axial degrees of freedom u_1 and u_2 . As evident from the $E_c A_g$ terms in Eq. (2), the axial behavior of the beam is assumed linear-elastic for simplicity.

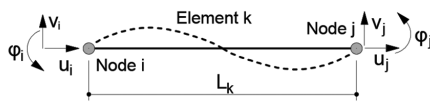
EXISTING ELEMENT FOR SLENDER BEAMS AND COLUMNS

1-D nonlinear elements for slender beams are employed by many nonlinear frame analysis platforms such as OpenSees,¹³ SAP2000,¹⁴ RUAUMOKO,¹⁵ VecTor5,¹⁶ and others. As shown in Fig. 4(a), beams and columns are discretized into several elements, and one element usually has two end nodes with three degrees of freedom per node (u, v, ϕ) as in the 1-D macroelement for deep beams discussed previously (Fig. 4(b)).

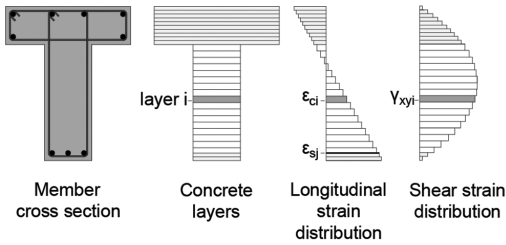
To model the nonlinear behavior of slender beams, this study focuses on the distributed plasticity approach. In this approach, the beam section is divided into a number of concrete and steel layers as shown in Fig. 4(b), and the longitudinal strains in the layers vary linearly across the section. The stresses in the layers are obtained from the strains based on material constitutive laws for uniaxial tension and compression. This is a universally accepted way of modeling flexural behavior, while the approaches for predicting the shear behavior vary significantly. For example, SAP2000¹⁴ and RUAUMOKO¹⁵ employ a lumped-plasticity approach where the locations and behavior of shear hinges is commonly defined by the user. However, expert knowledge on the shear behavior of concrete is required to define these shear hinges. In addition, the changing shear behavior as the elements sustain damage or axial force levels change cannot



(a) Beam modeling with slender elements



(b) Degrees of freedom



(c) Fiber-based sectional idealization

Fig. 4—Existing element for slender beams.

be captured. These severely limit the use of lumped-plasticity procedures for modeling shear effects in practice.

Shear behavior can also be modeled using a distributed plasticity approach, where the concrete layers do not work in uniaxial tension/compression, but under a 2-D state of stresses. This approach is more computationally demanding but removes the complex task of determining the shear hinge behavior from the user. VecTor5¹⁶ is one procedure based on a distributed plasticity approach and is adopted in this study. To simplify the problem, the pattern of distribution of the shear strains across the section is assumed either constant (not shown) or parabolic (shown in Fig. 4(c)). Knowing the longitudinal and shear strain distributions, each concrete and steel layer is analyzed individually based on the Distributed Stress Field Model (DSFM), Vecchio 2000.¹⁷ The DSFM is a smeared, hybrid crack model (that is, between a fully rotating and a fixed-crack model) and accounts for phenomena such as aggregate interlock; tension stiffening and softening; compression softening and confinement of the concrete; and yielding, strain hardening, buckling, and dowel action of the reinforcement. This approach has been evaluated with a large number of experiments showing adequate predictions as well as excellent convergence properties.¹⁸

MIXED-TYPE MODELING FRAMEWORK

The primary objective of this study is to propose an analysis framework, which integrates 1-D slender beam elements with a new 1-D macroelement for deep beams. A key advantage of the macroelement, which will permit achieving this objective, is that it uses the same nodal degrees of freedom as the 1-D slender elements.

The approach taken in this study is to avoid making major changes to the solution algorithm of the existing global analysis procedure of VecTor5. This is achieved by developing a new subroutine for the deep macroelement, which

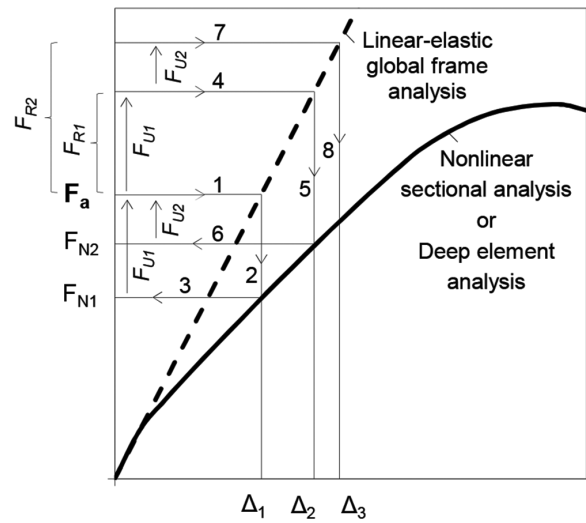


Fig. 5—Unbalanced force approach (adapted from Guner and Vecchio¹⁹).

performs the calculations discussed previously and returns the results of deep members to the global VecTor5 solution procedure. The unbalanced force approach used in VecTor5 (to be discussed in the following) ensures the compatibility of these results with those calculated for the slender elements. A major advantage of this approach is that no other changes (such as a new finite element development, solution algorithm changes, or degree of freedom modifications) are required for the global analysis procedure. Even though the proposed formulations are implemented in VecTor5 due to its robust shear behavior modeling, they are equally as applicable to other existing platforms for nonlinear analysis.

The unbalanced force method¹⁹ employed by VecTor5 is illustrated schematically in Fig. 5. The first step is to perform a global frame analysis with a constant stiffness under the applied loads $\{F_a\}$ to compute the nodal displacements Δ_1 (refer to path 1→2). These displacements are used to calculate the curvature and strain values for each element. The nonlinear sectional calculations are then performed, using the strain values, to obtain the end forces of the elements and the corresponding nodal forces for the entire structure F_{N1} (path 2→3). The difference between the applied forces and the nodal forces calculated by the sectional procedures are termed unbalanced forces $F_{U1} = F_a - F_{N1}$, which are used to establish a vector of the compatibility restoring forces $\{F_R\}$. These forces are applied in addition to the externally applied forces to increase the displacements and get closer to the true nonlinear response. Following this step, new unbalanced forces are calculated and added to $\{F_R\}$, and the iterations continue until all unbalanced forces converge to zero. This method is employed in VecTor5 for static analyses (such as monotonic and cyclic) as well as dynamic analyses (such as seismic, impact, or blast). This study focuses on the static monotonic (or pushover) analysis only.

The proposed mixed-type modeling framework based on the unbalanced force method is outlined in Fig. 6. In this flowchart, the steps related to the newly added subroutines for deep beam elements are shaded in grey. The subroutine for slender elements is presented very briefly within the existing VecTor5 procedure and is also shaded in grey. From

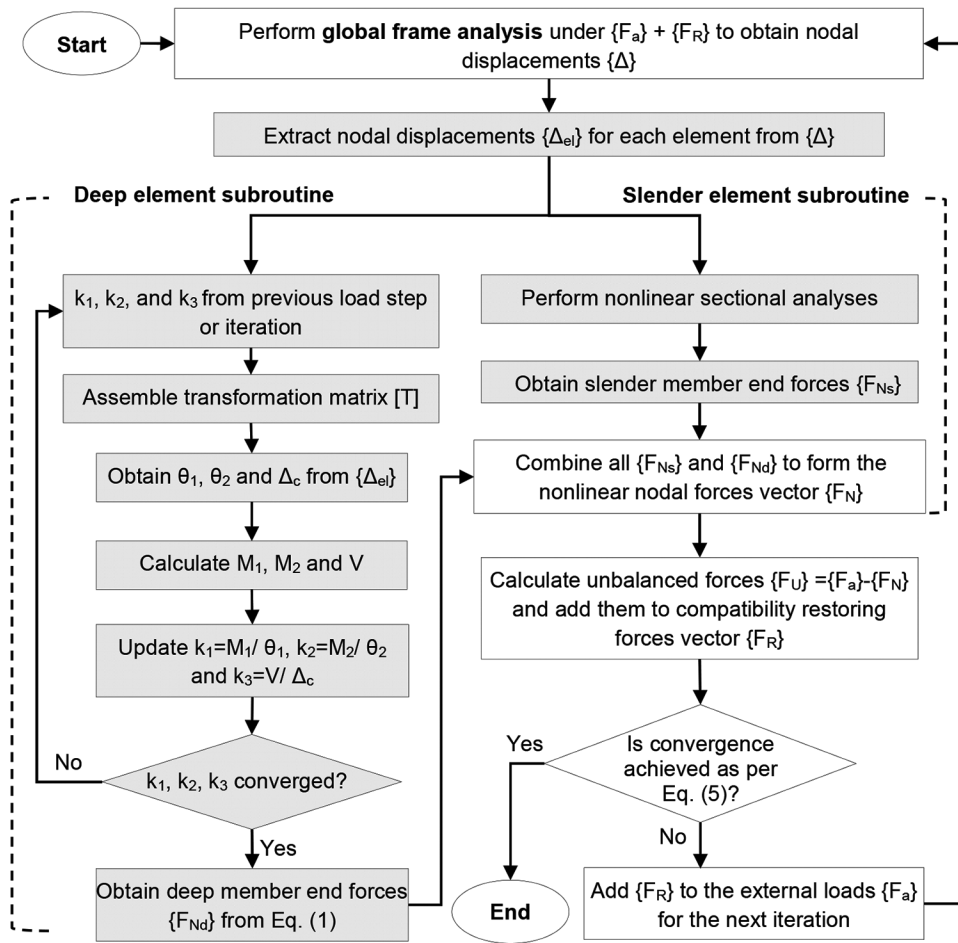


Fig. 6—Mixed-modeling framework.

the displacement vector $\{\Delta\}$, a subroutine extracts the nodal displacements of each element $\{\Delta_{el}\}$ and supplies them to the subroutines for either deep or slender elements. These subroutines perform nonlinear calculations under imposed $\{\Delta_{el}\}$ and return the member end forces $\{F_{Nd}\}$ and $\{F_{Ns}\}$. When assembled for the entire structure, $\{F_{Nd}\}$ and $\{F_{Ns}\}$ form the global vector of nodal forces, which is used by the unbalanced force method.

As illustrated in Fig. 6, the new subroutine for deep elements consists of six main steps. The calculations begin by obtaining the secant stiffnesses k_1 to k_3 of the three springs of the macroelement from the previous converged load step or previous iteration. In the first load step, the structure is elastic and the stiffness is obtained based on the Timoshenko's beam theory as detailed elsewhere.⁸ The internal degrees of freedom of the macroelement θ_1 , θ_2 , and Δ_c are then calculated under the imposed nodal DOFs $\{\Delta_{el}\}$. This is achieved through the use of a transformation matrix $[T]$ as follows

$$\begin{bmatrix} \theta_1 \\ \theta_2 \\ \Delta_c \end{bmatrix} = [T]\{\Delta\} = [T] \begin{bmatrix} u_1 \\ v_1 \\ \phi_1 \\ u_2 \\ v_2 \\ \phi_2 \end{bmatrix} \quad (3)$$

$$[T] = \frac{1}{k_1 + k_2 + k_3 a^2} \times \begin{bmatrix} 0 & -k_3 a & k_2 + k_3 a^2 & 0 & k_3 a & -k_2 \\ 0 & -k_3 a & -k_1 & 0 & k_3 a & k_1 + k_3 a^2 \\ 0 & k_1 + k_2 & -k_1 a & 0 & -(k_1 + k_2) & -k_2 a \end{bmatrix} \quad (4)$$

DOFs θ_1 , θ_2 , and Δ_c are used together with the nonlinear constitutive relationships of the springs (shown in Fig. 3) to obtain the end moments M_1 and M_2 as well as the shear V . As k_1 to k_3 are secant stiffnesses, they are recalculated as $k_1 = M_1/\theta_1$, $k_2 = M_2/\theta_2$, and $k_3 = V/\Delta_c$. The secant stiffness formulation always provides positive stiffness values and results in excellent convergence characteristics. The calculations are repeated until the initial and calculated stiffness values converge. The member end forces $\{F_{Nd}\}$ are then obtained from Eq. (1).

As mentioned previously, the obtained reaction forces $\{F_{Nd}\}$ and $\{F_{Ns}\}$ are assembled to form the global vector of nodal forces $\{F_N\}$. If forces $\{F_N\}$ are not equal to the applied forces $\{F_a\}$, unbalanced force will be calculated. The solution at a given load step is considered converged when the unbalanced forces are close to zero; otherwise, these forces are added to the vector of compatibility restoring forces $\{F_R\}$ from the previous iteration, and the entire procedure is repeated with the updated load $\{F_a\} + \{F_R\}$.

Table 1—Simply supported deep beam tests

Authors and year	Beam	a/d	b , mm	d , mm	h , mm	a , mm	L_f , mm	L , mm	l_{b1} , mm	l_{b2} , mm	f'_c , MPa	ρ_s , %	f_{ys} , MPa	ρ_v , %	f_{yv} , MPa	V_{exp} , kN	$V_{pred, 2D}$	$V_{pred, 1D}$
Tanimura and Sato 2005 ²¹	1	0.5	300	400	450	200	400	1400	100	100	23.2	2.14	458	0.00	—	853	1.08	1.06
	2	0.5	300	400	450	200	400	1400	100	100	23.2	2.14	458	0.21	370	821	1.08	1.00
	3	0.5	300	400	450	200	400	1400	100	100	23.2	2.14	458	0.48	388	833	1.09	1.02
	4	0.5	300	400	450	200	400	1400	100	100	23.2	2.14	458	0.84	368	869	1.15	1.07
	5	1.0	300	400	450	400	400	1800	100	100	29.0	2.14	458	0.00	—	632	0.94	1.14
	6	1.0	300	400	450	400	400	1800	100	100	29.1	2.14	458	0.21	370	731	1.00	1.23
	7	1.0	300	400	450	400	400	1800	100	100	29.2	2.14	458	0.48	388	750	0.97	1.20
	8	1.0	300	400	450	400	400	1800	100	100	29.3	2.14	458	0.84	368	804	0.91	1.23
	9	1.5	300	400	450	600	400	2200	100	100	22.9	2.14	458	0.00	—	284	0.78	0.80
	10	1.5	300	400	450	600	400	2200	100	100	22.5	2.14	458	0.21	370	464	0.94	1.13
	11	1.5	300	400	450	600	400	2200	100	100	23.0	2.14	458	0.48	388	491	0.84	0.99
	12	1.5	300	400	450	600	400	2200	100	100	23.5	2.14	458	0.84	368	570	0.92	0.99
Salamy et al. 2005 ²²	B-10-2	1.5	240	400	475	600	300	1900	100	100	23.0	2.02	376	0.00	—	357	1.08	1.41
	B-13-2	1.5	480	800	905	1200	600	3800	200	200	24.0	2.07	398	0.00	—	1128	1.00	1.10
	B17	1.5	600	1000	1105	1500	750	4750	250	250	28.7	2.04	398	0.40	398	2607	0.98	1.09
	B15	1.5	720	1200	1305	1800	900	5700	300		27.0	1.99	402	0.00	—	2695	1.06	1.16
	B18	1.5	840	1400	1505	2100	1050	6650	350		23.5	2.05	398	0.40	398	4198	0.89	0.95
																Avg	0.98	1.09
																COV	10.1%	12.6%

Notes: 1 mm = 0.039 in.; 1 MPa = 145.038 psi; 1 kN= 0.225 kip.

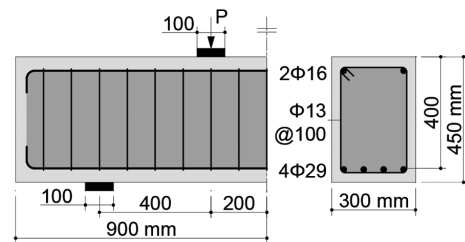
EVALUATION AND APPLICATIONS

To evaluate the new mixed-type modeling framework with experimental results, 17 simply supported deep beams, one continuous deep beam, and one large frame structure are analyzed. All beams were shear-critical and modeled with both the proposed 1-D mixed-type modeling approach and a 2-D high-fidelity finite element model (FEM). The 2-D FEM analyses are performed with program VecTor2²⁰ based on the same theory (that is, the DSFM¹⁷) as in VecTor5 to avoid discrepancies related to the theories used in the global analyses. The two modeling approaches are compared in terms of accuracy and computational efficiency.

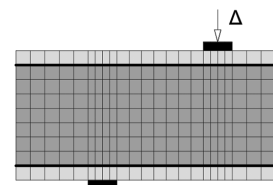
Simply supported deep beams

The simply supported deep beams considered in this study were tested to failure by Tanimura and Sato²¹ (12 beams) and Salamy et al.²² (five beams). All beams were subjected to symmetrical four-point bending and featured different geometry and material properties as listed in Table 1. The shear span-depth ratio a/d varied from 0.5 to 1.5, the effective depth from 400 to 1400 mm (15.75 to 55.12 in.), the longitudinal reinforcement ratio from 1.99% to 2.14%, the stirrup ratio from 0 to 0.84%, and the concrete compressive strength from 22.5 to 29.3 MPa (3263 to 4250 psi).

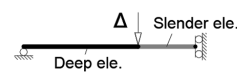
A representative sample beam (for example, Beam 8 in Table 1) and the two models created for this beam are shown in Fig. 7. The FEM consists of quadrilateral elements for the concrete and discrete truss elements for the longitudinal reinforcement. As the stirrups are typically uniformly spaced, they are modeled with smeared reinforcement as a



a) Deep beam under symmetrical 4-point bending⁹



b) 2D finite element model



c) 1D mixed-type model

Fig. 7—Modeling of simply supported deep beam 8. (Note: 1 mm = 0.039 in.)

part of the concrete elements. To allow the analyses to be easily repeated by others, the default constitutive models of VecTor2 were used with no tuning of any input parameters. The only exception is the compression stress-strain

curve of the concrete for which the Popovics²³ model was preferred over the default simple parabola. The beams are analyzed under imposed increasing displacements applied at the loading points.

In contrast to the 2-D FEM that uses 261 elements for Beam 8, it can be seen in Fig. 7(c) that the proposed 1-D mixed-type modeling approach uses only two elements for the same beam. A slender element is used for the pure bending region while a deep macroelement is used for the shear span to show the compatibility of the two elements in the same structure. Again, the default constitutive models of VecTor5 were used (except for the compression stress-strain curve of the concrete), which are the same as those contained in VecTor2, to achieve a more consistent comparison.

To verify the proposed modeling approach, it is first necessary to examine its convergence properties. For this study, an unbalanced-force-based-convergence criterion is used as follows

$$CF = 1 + \sqrt{\frac{1}{3 \times n} \times \sum_{i=1}^n \left(\left(\frac{N_{ui}}{N_i} \right)^2 + \left(\frac{V_{ui}}{V_i} \right)^2 + \left(\frac{M_{ui}}{M_i} \right)^2 \right)} \quad (5)$$

where n is the total number of elements; N_{ui} , V_{ui} , and M_{ui} are the unbalanced end forces for each element; and N_i , V_i , and M_i are the end element forces calculated by the global frame analysis. The convergence factors CF and the number of iterations from the analysis of Beam 8 are plotted in Fig. 8 as functions of the load step number, where the peak resistance of the beam was reached at load step 19. It can be seen that the solution reached convergence at all load steps, including in the post-peak regime of the beam. This was achieved even without reaching the maximum number of iterations (that is, 100). Similar observations were made for the rest of the beams modeled in this study.

The complete pre- and post-peak load-deflection responses of the seventeen simply supported deep beams in Table 1 are shown in Fig. 9. The plots compare the experimentally obtained responses to the predictions from the 1-D (proposed) and 2-D models. Overall, both approaches capture the pre-peak response and produce satisfactory strength predictions within $\pm 10\%$ —well inside the margins of error expected when analyzing shear-critical reinforced concrete members. As shown in Table 1, the average shear strength experimental-to-predicted ratio obtained with the 2-D FEM is 0.98 and the coefficient of variation (COV) is 10.1%. For the proposed 1-D mixed-type modeling approach, these numbers are respectively 1.09 and 12.6%, which indicates that the new approach is slightly more conservative than the 2-D FEM. It can also be observed in Fig. 9 that the 1-D model produced better results in the post-peak regime, which becomes very important when evaluating the resilience of structures under extreme loads. While the 2-D FEM predicts very brittle failures, the proposed 1-D model accounts for the available residual capacity. Therefore, the new modeling framework will be able to properly account for the redistribution of forces in complex statically indeterminate structures incorporating deep beams.

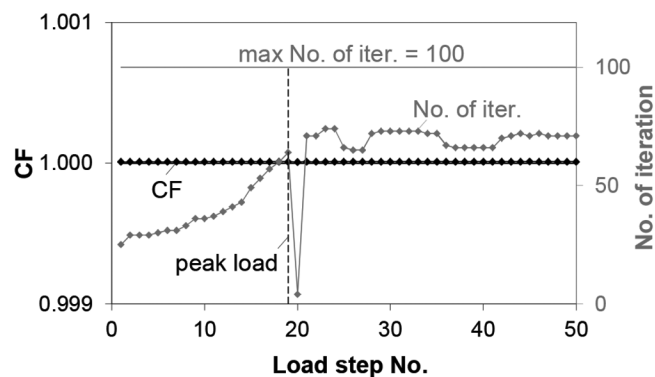


Fig. 8—Convergence during analysis of Beam 8.

To better understand the modeling of the peak and post-peak behavior, Fig. 10 compares measured and predicted crack and deformation patterns of two specimens. In Beams 1 and B-15 with a/d of 0.5 and 1.5, respectively, the critical shear cracks developed diagonally across the shear span. For the shorter beam (that is, Beam 1), the 1-D and 2-D models produce very similar deformation patterns at failure. For the longer beam (that is, Beam B-15), the 1-D model uses a straight diagonal crack while the 2-D model predicts a steeper critical crack that extends along the bottom reinforcement. To generate these patterns, the 1-D model uses DOFs θ_1 and Δ_c ($\theta_2 = 0$ as the shear span is under single curvature bending), while the 2-D model uses several hundreds of DOFs. Furthermore, as the proposed simpler approach models a discrete critical crack, it can accurately capture the ductility of the member when large sliding displacements occur along the crack in the post-peak regime. In contrast, the 2-D smeared crack formulation results in a large concentration of principal tensile strains in a narrow band of finite elements. These strains in turn result in unrealistically high compression softening of the concrete and a rapid loss of post-peak resistance. Similar observations have been made with other 2-D smeared crack formulations, as they all result in strain concentrations (refer to, for example, the predictions of platform DIANA for Beam B-15 in Fig. 9 reported by Salamy et al.²¹).

It is also of interest to compare the analysis time required by the 1-D and 2-D models. On the same PC with a 3.4 GHz quad-core processor and 16 GB of RAM, the 1-D model required an average analysis time (considering all 17 beams) of approximately 5 seconds, while the 2-D model required approximately 50 seconds. While both times are short, the difference between the two models becomes important when large structures are analyzed as it will be demonstrated later. In addition, the time for modeling with the 1-D approach is significantly shorter due to the straightforward input and small number of elements required.

Continuous deep beams

A continuous deep beam with two symmetrical spans was tested under two symmetrical concentrated loads by Mihaylov et al.¹¹ (refer to Fig. 11). The beam had a symmetrical top and bottom longitudinal reinforcement with a ratio of 0.91%, as well as stirrups with a ratio of 0.20%. As shown in Fig. 11(b) and (c), only one-half of the beam was modeled

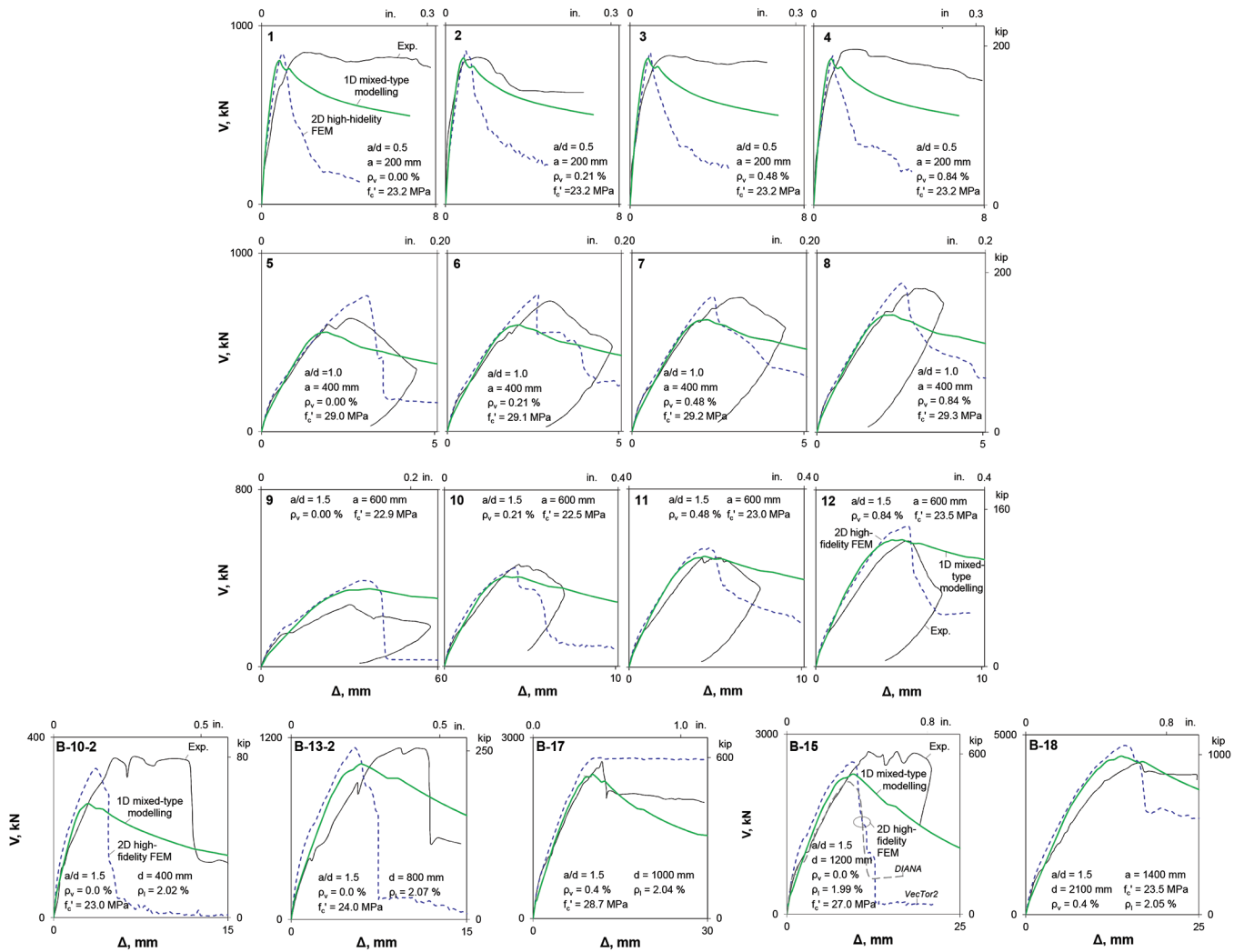


Fig. 9—Measured and predicted load-displacement response of simply supported deep beams. (Note: 1 mm = 0.039 in.; 1 MPa = 145 psi.)

due to the symmetry. The 2-D FEM uses 1179 elements while the proposed 1-D model uses only two macroelements. The two macroelements model the two shear spans, where the external shear span is under single curvature and the internal one is under double curvature. As with the simply supported beams, significantly less time was needed to generate the 1-D model as compared to the 2-D FEM. In terms of analysis time, the 2-D model required approximately 145 seconds, while the 1-D model took approximately 3 seconds to complete the calculations.

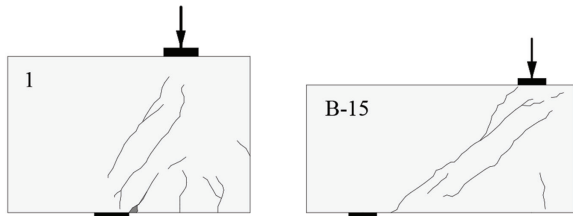
Figure 12 shows the measured and predicted load-deflection responses of the continuous deep beam. The three curves correspond to the applied load P , the shear in the external shear span V_{ext} and the shear in the internal shear span V_{int} . These three forces were measured in the test and illustrate the fundamental differences between simply supported and continuous deep beams. It can be seen that the internal shear span attracted more shear and reached its peak shear resistance at a deflection of approximately 3.5 mm (0.14 in.). However, due to the statical indeterminacy of the beam, as the resistance of the critical shear span decreased, the shear was redistributed towards the external shear span. This resulted in a significant global ductility of the member even though the beam failed in shear without yielding of the

longitudinal reinforcement. As evident from Fig. 12, this ductility is captured well by the proposed 1-D model, while the 2-D FEM slightly underestimates the ability of the beam to deform plastically in the post-peak regime. In contrast, in the pre-peak regime, the 2-D model provides better stiffness predictions. The lower stiffness obtained from the 1-D element stems from the fact that, for simplicity, the macroelement is assumed fully cracked from the beginning of the loading, while the full formulation of the macroelement with an initial uncracked response is described elsewhere.⁸

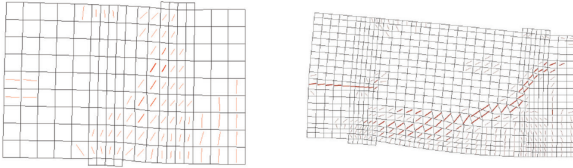
Frame structure

Finally, it is of interest to compare the different modeling approaches when analyzing large frame structure containing both slender and deep members. As laboratory tests of such structures are not available even in small scales, a sample 20-story frame was designed based on the ACI 318 provisions.²⁴ Figure 13 shows the bottom two stories of the frame where a deep transfer girder is used to support a column from the floors above. The depth of the girder is chosen as 1.8 m (5.9 ft), resulting in an a/d of 1.63.

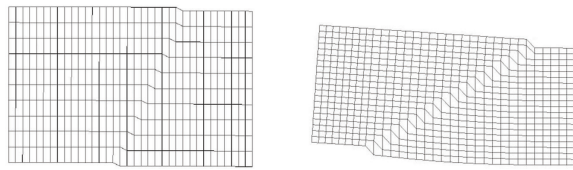
The lowermost two floors were modeled based on two strategies: 2-D FEM and proposed 1-D mixed-type modeling approach (Fig. 14(a) and (b)). The latter approach was also



a) Observed cracks at failure

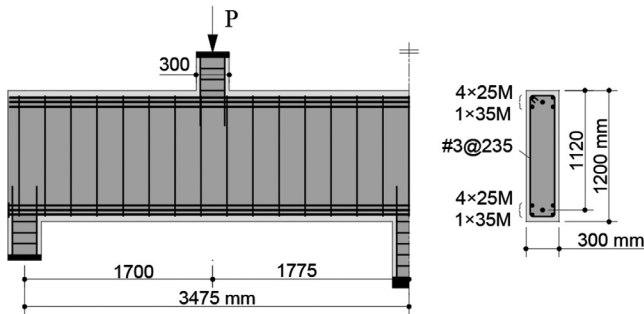


b) 2D FEM predictions at failure (displacements $\times 20$)

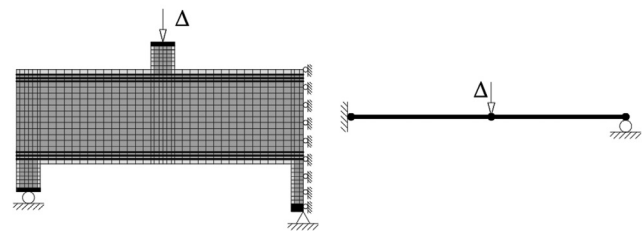


c) 1D mixed-type model predictions at failure ($\times 20$)

Fig. 10—Crack and deformation patterns of Beams 1 and B-15.



a) Continuous deep beam specimen



b) 2D FE model

c) 1D mixed-type model

Fig. 11—Modeling of continuous deep beam tested by Mihaylov et al. (Note: 1 mm = 0.039 in.)

used to model the entire 20-story frame (Fig. 14(c)). For simplicity, only three-point loads were applied at the top beam-column joints in the two-story models. The loads were increased monotonically until the transfer girder failed in shear along diagonal cracks.

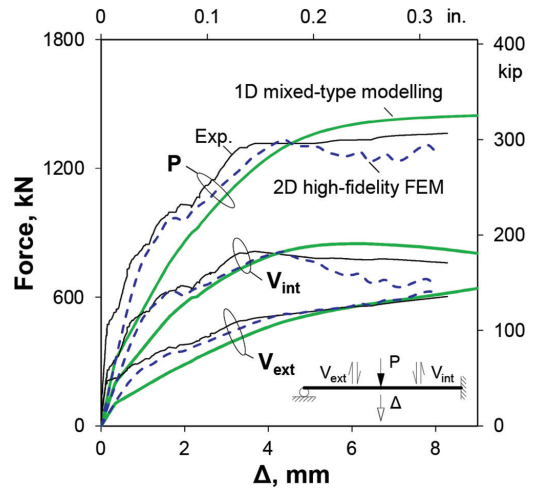


Fig. 12—Measured and predicted load-displacement response of continuous deep beam.

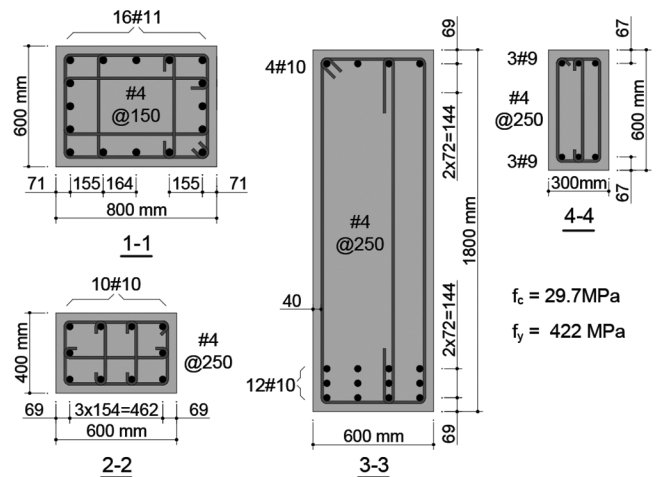
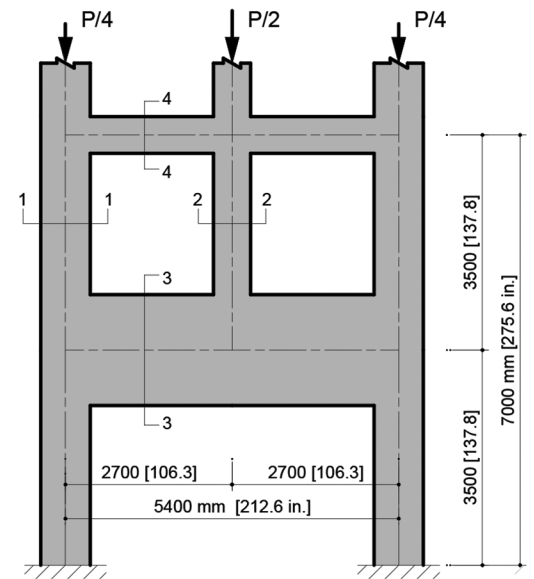


Fig. 13—Two-story single-span frame. (Note: 1 mm = 0.039 in.; 1 MPa = 145.04 psi.)

The total applied load on the frame is plotted in Fig. 15 as a function of the deflection of the deep transfer girder. As evident from the plot, the 2-D FEM and the 1-D mixed-type

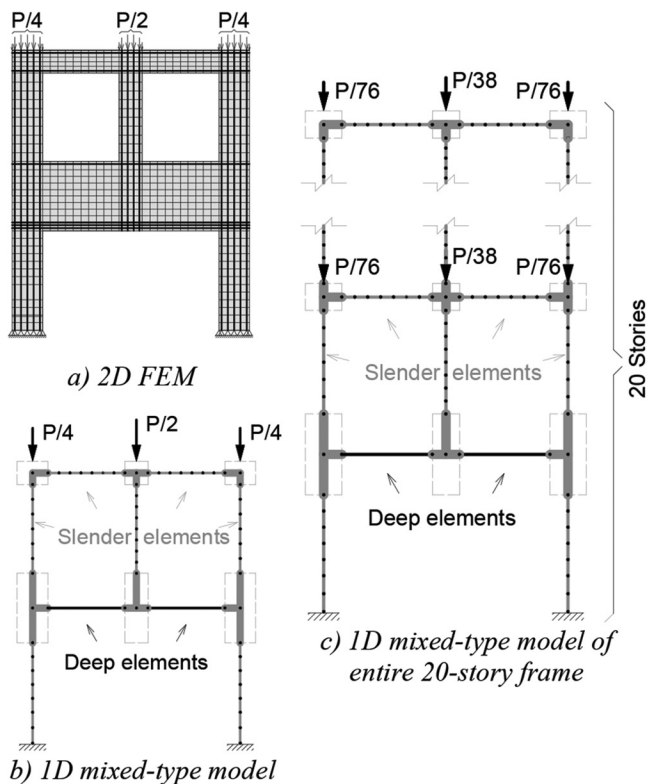


Fig. 14—Modeling of 12-story frame.

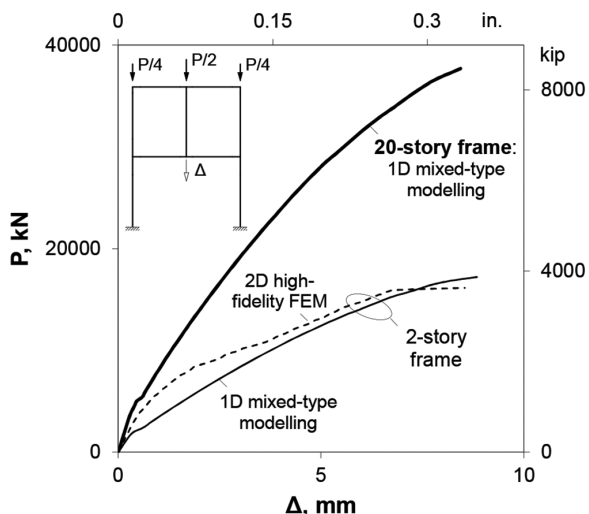


Fig. 15—Load-deflection results from frame analysis under applied vertical loads.

modeling approach produced very similar results, including an almost identical peak load. The plot also shows the results from the complete analysis of the 20-story frame performed with the 1-D model in Fig. 14(c). The forces $P/2$ and $P/4$ applied in the two-story model were distributed as $P/38$ and $P/76$ along the height of the 20-story model. Therefore, the load P in Fig. 15 remains the total load on the frame. In this regard, it is of interest to note that the 20-story building carried nearly two times larger total load than the two-story frame. This increased resistance is due to the slender beams in the above floors which, though significantly less stiff than the transfer girder, provide a certain resistance as the girder deforms and fails in shear. Therefore, focusing the analysis

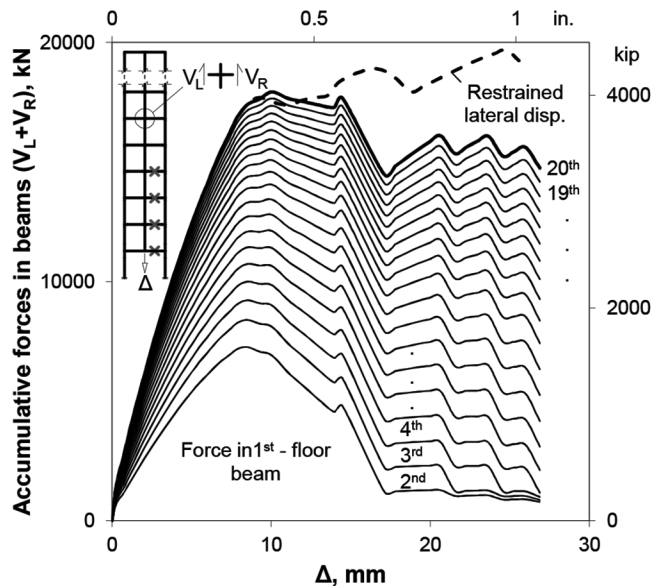


Fig. 16—Load-deflection results from frame analysis under applied vertical displacements.

on the bottom two floors and neglecting the interaction with the slender beams in the higher floors proves to be very conservative in this case.

To further study the redistribution of forces between deep and slender beams, an additional analysis of the 20-story frame is performed under imposed displacements. As shown in the inset of Fig. 16, equal vertical displacements were applied at the internal beam-column joints to obtain the post-peak behavior of the frame. The plot shows the accumulative vertical force resulting from the shear forces in each beam. It can be seen that at the peak load the transfer girder carries approximately 40% of the total load. In the post-peak regime, the deep girder fails almost completely when the deflection reaches approximately 18 mm (0.71 in.), followed by the consecutive shear failures of the slender beams in the second, third, and fourth floors. All failures occur in the same bay and the frames displace laterally. Regardless of these failures, the structure continues to support a significant portion of the peak load due to the redistribution of the forces among the beams.

A final analysis shows that the ductility of the frame can be further improved if it is part of a structure with stiff shear walls. The walls will limit the lateral displacements of the frame in the post-peak regime and will force more symmetrical shear failures in the two bays. The dashed line in Fig. 16 shows the behavior of the frame when the lateral displacements are fully restrained. It can be seen that while the pre-peak response remains unchanged, the post-peak resistance is significantly higher, and therefore the structure is more resilient to overloading. This highlights the need for efficient 1-D models for slender and deep beams that allow to capture the favorable effects that develop at the global structural level.

Efficiency of studied modeling strategies

Finally, the efficiency of the proposed 1-D mixed-type modeling framework is examined and graphically illustrated

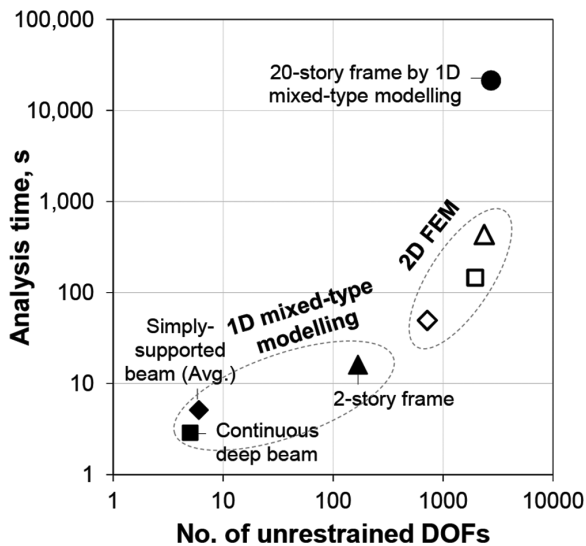


Fig. 17—Efficiency of modeling strategies.

in Fig. 17. The plot shows that for the structures modeled in this study, the proposed 1-D model required significantly fewer degrees of freedom and computational time than the 2-D FEM. The largest model (that is, the 20-story frame under imposed displacements) required slightly less than 6 hours with 40 load steps. While not attempted, the analysis of this frame with the 2-D FEM would require many days to run. In addition, creating a finite element mesh would require significant time and experience. This advantage of the proposed 1-D mixed-type modeling will be even more pronounced in the analysis of larger multi-bay multi-story structures.

CONCLUSIONS

This paper proposed a novel mixed-type modeling framework for large structures containing both slender and deep members. The framework integrates existing 1-D beam elements for slender members with a 1-D macroelement for shear spans of deep beams. It was implemented in an existing computer program VecTor5 for monotonic loading conditions, and evaluated with 18 deep beams and a 20-story frame. The performed studies led to the following conclusions:

1. The 1-D macroelement for deep shear spans provides a full compatibility with fiber-based 1-D beam elements for slender members as it uses the same nodal DOFs.
2. When applied to simply supported deep beams, the proposed framework produces similarly adequate results as those obtained with 2-D high-fidelity FEM, and even improves the post-peak predictions.
3. The proposed mixed-type modeling framework uses straightforward input and requires significantly less time for modeling and computation than 2-D FEM.
4. As the new framework is computationally efficient and captures well the complete pre- and post-peak behavior of frames with slender and deep members, it represents a valuable tool for the analysis of complex structures under extreme loading.

AUTHOR BIOS

ACI member **Jian Liu** is a PhD Student in the Department of ArGenCo at the University of Liege, Liege, Belgium. She received her MSc from the Erasmus Mundus Program in earthquake engineering and engineering seismology (MEEES) in 2013. Her research interests include shear behavior of reinforced concrete deep beams.

ACI member **Serhan Guner** is an Assistant Professor in the Department of Civil Engineering at the University of Toledo, Toledo, OH. He received his PhD from the University of Toronto, Toronto, ON, Canada. He is a member of Joint ACI-ASCE Committee 447, Finite Element Analysis of Reinforced Concrete. His research interests include finite element modeling of reinforced concrete structures; shear effects in concrete; development of analysis software; and structural response to impact, blast, and seismic loads.

ACI member **Boyan I. Mihaylov** is an Assistant Professor of civil engineering at the University of Liege. He received his PhD from the University of Pavia, Pavia, Italy in 2009 and was Postdoctoral Fellow at the University of Toronto until 2013. His research interests include shear design of deep members and the development of macrokinematic approaches for the shear behavior of disturbed concrete regions and members.

NOTATION

A_g	=	gross area of cross section
a	=	shear span
a/d	=	shear-span-to-effective-depth ratio
b	=	cross section width
d	=	effective depth of section with respect to bottom reinforcement
E_c	=	modulus of elasticity of concrete
f'_c	=	concrete cylinder strength
f_y	=	yield strength of longitudinal reinforcement
f_{yv}	=	yield strength of stirrups
$\{F_a\}$	=	vector of applied loads
$\{F_N\}$	=	vector of nodal forces for all members from nonlinear procedures
$\{F_{Nd}\}$	=	vector of deep member end forces from nonlinear procedure
$\{F_{Ns}\}$	=	vector of slender member end forces from nonlinear procedure
$\{F_R\}$	=	vector of compatibility restoring forces
$\{F_U\}$	=	vector of unbalanced forces
h	=	total depth of section
$[k]$	=	secant stiffness matrix of macroelement
$k_{1/2}$	=	secant stiffness of rotational spring 1/2
k_3	=	secant stiffness of transverse spring
L	=	beam length
L_f	=	distance between two loading points
l_{b1}	=	width of loading plate parallel to longitudinal axis of member
l_{b2}	=	width of support plate parallel to longitudinal axis of member
$M_{1/2}$	=	bending moment at end section 1/2
$N_{1/2}$	=	axial force at end section 1/2
P	=	total force applied to frame structure
$P_{1/2}$	=	applied concentrated load or support reaction
$T_{1/2}$	=	tension force in bottom/top longitudinal reinforcement
$[T]$	=	transformation matrix relating nodal displacements to internal DOFs of macroelement
$u_{1/2}$	=	axial displacement of end section 1/2
$V_{1/2}$	=	shear force at end section 1/2
V_{CLZ}	=	shear resisted by critical loading zone
V_{ci}	=	shear resisted by aggregate interlock
V_d	=	shear resisted by dowel action
V_{exp}	=	measured shear capacity
$V_{ext/int}$	=	shear force in the external/internal shear spans of continuous deep beams
$V_{pred,1D}$	=	shear capacity predicted by 1-D mixed-type model
$V_{pred,2D}$	=	shear capacity predicted by 2-D high-fidelity FEM
V_s	=	shear resisted by stirrups
$v_{1/2}$	=	transverse displacement of end section 1/2
$\{\Delta\}$	=	vector of nodal displacements from global frame analysis
Δ_c	=	transverse displacement of CLZ
$\{\Delta_{el}\}$	=	vector of nodal displacements for each element
$\epsilon_{t1/2,avg}$	=	average strain along bottom/top longitudinal reinforcement
$\phi_{1/2}$	=	rotation of end section 1/2
$\theta_{1/2}$	=	opening of fan 1/2
ρ_l	=	ratio of bottom longitudinal reinforcement
ρ_v	=	stirrup ratio

REFERENCES

1. Goldsworthy, H. M., "Lessons on Building Design from the 22 February 2011 Christchurch Earthquake," *Australian Journal of Structural Engineering*, V. 13, No. 2, 2012, pp. 159-173. doi: 10.7158/S11-136.2012.13.2
2. Elwood, K. J., "Performance of Concrete Buildings in the 22 February 2011 Christchurch Earthquake and Implications for Canadian Codes," *Canadian Journal of Civil Engineering*, V. 40, No. 3, 2013, pp. 759-776. doi: 10.1139/cjce-2011-0564
3. Kam, W. Y.; Pampanin, S.; and Elwood, K., "Seismic Performance of Reinforced Concrete Buildings in the 22 February Christchurch (Lyttelton) Earthquake," *Bulletin of the New Zealand Society for Earthquake Engineering*, V. 44, No. 4, 2011, pp. 239-278.
4. Canterbury Earthquakes Royal Commission, V. 4, Final Report Part Two, Earthquake-Prone Buildings, 2012. <https://canterbury.royalcommission.govt.nz/Final-Report---Part-Two>. (last accessed June 12, 2019)
5. Guner, S., "Performance Assessment of Shear-Critical Reinforced Concrete Plane Frames," doctoral thesis, University of Toronto, Toronto, ON, Canada, 2008.
6. Rombach, G. A., *Finite Element Design of Concrete Structures: Practical Problems and Their Solution*, Thomas Telford, London, UK, 2004.
7. Sadeghian, V.; Vecchio, F. J.; and Kwon, O., "An Integrated Framework for Analysis of Mixed-Type Reinforced Concrete Structures," *CompDyn 2015 Conference*, 2015.
8. Liu, J., and Mihaylov, B. I., "Macroelement for Complete Shear Behavior of Continuous Deep Girders," *ACI Structural Journal*, V. 115, No. 4, July 2018, pp. 1089-1099. doi: 10.14359/51702047
9. Mihaylov, B. I.; Hunt, B.; Bentz, E. C.; and Collins, M. P., "Three-Parameter Kinematic Theory for Shear Behavior of Continuous Deep Beams," *ACI Structural Journal*, V. 112, No. 1, Jan.-Feb. 2015, pp. 47-57. doi: 10.14359/51687180
10. AASHTO, "AASHTO LRFD Bridge Design Specifications," fourth edition, American Association of State Highway Officials, Washington, DC, 2007, pp. 1526.
11. Mihaylov, B. I.; Bentz, E. C.; and Collins, M. P., "Behavior of Large Deep Beams Subjected to Monotonic and Reversed Cyclic Shear," *ACI Structural Journal*, V. 107, No. 6, Nov.-Dec. 2010, pp. 726-734.
12. Li, B.; Maekawa, K.; and Okamura, H., "Contact Density Model for Stress Transfer across Cracks in Concrete," *Journal of the Faculty of Engineering, University of Tokyo*, V. 40, No. 1, 1989, pp. 9-52.
13. Mazzoni, S.; McKenna, F.; Scott, M. H.; and Fenves, G. L., "Open System for Earthquake Engineering Simulation: User Command-Language Manual," Pacific Earthquake Engineering Research Center, University of California, Berkeley, OpenSees version 2.0 users' manual, <http://opensees.berkeley.edu/OpenSees/manuals/usermanual/index.html>, May 2009.
14. Computers and Structures, Inc., "CSI Analysis Reference Manual for SAP2000®, ETABS®, SAFE® and CSiBridge®," Berkeley, CA, 2016.
15. Carr, A., *Ruamoko Theory Manual*, University of Canterbury, Christchurch, New Zealand, 2015.
16. Guner, S., and Vecchio, F. J., *User's Manual of VecTor5*, documentation, 2008, 88 pp.
17. Vecchio, F. J., "Disturbed Stress Field Model for Reinforced Concrete: Formulation," *Journal of Structural Engineering*, ASCE, V. 126, No. 9, 2000, pp. 1070-1077. doi: 10.1061/(ASCE)0733-9445(2000)126:9(1070)
18. Guner, S., and Vecchio, F. J., "Pushover Analysis of Shear-Critical Frames: Verification and Application," *ACI Structural Journal*, V. 107, No. 1, Jan.-Feb. 2010, pp. 72-81.
19. Guner, S., and Vecchio, F. J., "Pushover Analysis of Shear-Critical Frames: Formulation," *ACI Structural Journal*, V. 107, No. 1, Jan.-Feb. 2010, pp. 63-71.
20. Wong, P. S.; Vecchio, F. J.; and Trommels, H., *VecTor2 & FormWorks User's Manual*, second edition, University of Toronto, Toronto, ON, Canada, 2013.
21. Tanimura, Y., and Sato, T., "Evaluation of Shear Strength of Deep Beams with Stirrups," *Quarterly Report of RTRI*, V. 46, No. 1, 2005, pp. 53-58. doi: 10.2219/rtriq.46.53
22. Salmay, M. R.; Kobayashi, H.; and Unjoh, S., "Experimental and Analytical Study on RC Deep Beams," *Asian Journal of Civil Engineering*, V. 6, No. 5, 2005, pp. 409-421.
23. Popovics, S., "A Review of Stress-Strain Relationships for Concrete," *ACI Journal Proceedings*, V. 67, No. 3, Mar. 1970, pp. 243-248.
24. ACI Committee 318, "Building Code Requirements for Structural Concrete (ACI 318-14) and Commentary (ACI 318R-14)," American Concrete Institute, Farmington Hills, MI, 2014, 519 pp.